fit (smooth lines) for the two most highly displaced modes, ν_1, and ν_2, are shown in the inset of Figure 13.

In the process of excitation into the lowest allowed electronic transition of $Rh_2(O_2CCH_3)_4L_2$, where L = PPh_3 or $AsPh_3$, the largest bond length changes occur along the Rh-Rh and Rh-O bonds. The Rh-Rh bond length change in $Rh_2(O_2CCH_3)_4L_2$ is 0.047 Å for L = PPh_3 and 0.042 Å for L = $AsPh_3$. The Rh-O bond length change in $Rh_2(O_2CCH_3)_4L_2$ is 0.035 Å for L = PPh_3 and 0.041 Å for L = $AsPh_3$. There are also many modes that show small bond length or angle changes upon this excitation: for example, the C-O-C angle bend and the modes primarily involving phenyl rings. The O-C-O bond angle change in $Rh_2(O_2CCH_3)_4L_2$ is 0.46° for L = PPh_3 and 0.92° for L = $AsPh_3$. The magnitude of the change in the Rh-O bond on transition to an electronic state that is considered to be σ^*(Rh-Rh) is surprising. However, the metal d_{z^2} orbital which is the major component of the Rh-Rh σ interaction is also σ antibonding with respect to the oxygen atoms. Therefore, the $\sigma \rightarrow \sigma^*$ transition would be expected to change the net Rh-O bond and thus cause the displacement of the ν(Rh-O) normal coordinate. In addition, the significant displacement suggests that the resonant transition must also have RhO character to it, presumably via π(RhO) $\leftarrow d_{xy}$, π(RhO) $\leftarrow d_{xz}$, d_{yz}, and σ(RhO) $\leftarrow d_{z^2}$ parentage.

5. Summary

From the time-dependent point of view, the Raman intensities are governed by the overlap of the time-dependent wave packet with the final Raman wave function of interest as a function of time. The critical physical factors are the magnitude of the overlap and the time development of the overlap. The magnitude of the overlap for a fundamental is larger than that for overtones. The magnitude of a combination band is smaller than those of the fundamentals of the modes comprising the combination band. The time development of the overlap depends on both the frequency of the vibration and the displacement of the potential surface along the normal coordinate. The higher the frequency or the greater the displacement, the faster the time development. The overlaps of fundamentals develop faster in time than those of overtones. The damping of the overlap determines whether short-time or long-time processes dominate the intensities. For large molecules where short-time processes dominate, the larger the initial overlap and the faster the overlap increases with time, the higher the Raman intensity.

The resonance Raman spectrum of $W(CO)_5(py)$ was calculated. The calculated displacements are in excellent agreement with those determined in the analysis of the MIME. Both the excitation profiles and the resonance Raman spectra of $Rh_2(O_2CCH_3)_4L_2$, where L = PPh_3 or $AsPh_3$, have been accurately calculated. These molecules have significant displacements in the Rh-Rh and Rh-O normal coordinates.

Acknowledgment. This work was made possible by a grant from the National Science Foundation (CHE88-06775).

Contribution from the Department of Chemistry,
Northern Illinois University, DeKalb, Illinois 60115

Electronic Absorption and MCD Spectra for the Binuclear Three-Coordinate Gold(I) Complex $Au_2(dmpm)_3^{2+}$ (dmpm = Bis(dimethylphosphino)methane)

Huey-Rong C. Jaw, M. Meral Savas, and W. Roy Mason*

Received February 22, 1989

Electronic absorption and magnetic circular dichroism (MCD) spectra are reported for $[Au_2(dmpm)_3](ClO_4)_2$ in H_2O and CH_3CN solution in the region 2.5-5.2 μm^{-1}. Thin-film absorption spectra at 300 and 77 K are also reported for $[Au_2(dmpm)_3]Cl_2$ dissolved in polymerized poly(vinyl alcohol) (PVA). An intense band observed at 3.91 μm^{-1} is assigned as the Au_2-localized $d\sigma^* \rightarrow p\sigma$ transition of predominantly singlet character. The equivalent MCD band is weak and poorly resolved, a result that is interpreted in terms of orbital symmetry restrictions on the magnetic mixing of the excited state with close-lying states (*B*-term interactions). Two weaker bands to the red side of the spectrum are assigned to transitions to $d\sigma^* \rightarrow p\sigma$ and $d\delta \rightarrow p\sigma$ spin-orbit states of triplet parentage. At higher energy two poorly resolved intense bands are observed characterized by a strong positive *A* term in the MCD spectrum near 5.1 μm^{-1}. These bands are interpreted as due to transitions localized mainly within the AuP_3 unit. The spectroscopic results are compared with studies of related complexes.

Introduction

The binuclear gold(I) cation $Au_2(dmpm)_3^{2+}$ (dmpm = bis(dimethylphosphino)methane) has an interesting trigonal structure that consists of two nearly planar AuP_3 units linked by bridging dmpm ligands in a parallel face to face configuration. The Au-Au vector lies along the molecular C_3 axis and features a relatively short Au-Au distance (3.050 (1) Å in the BF_4^- salt).[1] The closed-shell $5d^{10}$-$5d^{10}$ electron configuration is formally nonbonding between the Au(I) ions, but the close Au-Au contact compared to the van der Waals distance (~3.4 Å)[2] indicates a significant Au-Au interaction. Short Au-Au contacts are found in other binuclear Au(I) complexes,[3,4] including the related $Au_2(dmpm)_2^{2+}$ cation (two linear AuP_2 units bridged parallel to one another with Au-Au = 3.028 (2) Å), which has been investigated extensively in our laboratory recently. The trigonal three-coordination of the Au(I) ions in the $Au_2(dmpm)_3^{2+}$ cation is less common than the linear two-coordination of $Au_2(dmpm)_2^{2+}$ and is believed to be responsible for several differences in their electronic absorption and magnetic circular dichroism (MCD) spectra in the UV region.[5] These features together with a recent report[6] of electronic spectra for the structurally similar nd^{10}-nd^{10} binuclear complexes $M_2(dppm)_3$ (M = Pd(0), Pt(0); dppm = bis(diphenylphosphino)methane) provided motivation for the present report of our spectroscopic studies of the $Au_2(dmpm)_3^{2+}$ cation. This paper reports room-temperature solution absorption and MCD spectra for $[Au_2(dmpm)_3](ClO_4)_2$ in water and acetonitrile in the region 2.5-5.2 μm^{-1} and absorption spectra for $[Au_2(dmpm)_3]Cl_2$ at 300 and 77 K in thin films of solid poly(vinyl alcohol) (PVA).

Experimental Section

Preparation of $Au_2(dmpm)_3^{2+}$ Salts. Bis(dimethylphosphino)methane, $(CH_3)_2PCH_2P(CH_3)_2$, was purchased from Strem Chemicals Co. and

(1) Bensch, W.; Prelati, M.; Ludwig, W. *J. Chem. Soc., Chem. Commun.* **1986**, 1762.
(2) Bondi, A. *J. Phys. Chem.* **1964**, *68*, 441.
(3) Puddephatt, R. J. *Comprehensive Coordination Chemistry*; Wilkinson, G., Gillard, R. D., McCleverty, J. A., Eds.; Pergamon Press: Oxford, England, 1987; Vol. 5, p 861.
(4) Jaw, H.-R. C.; Savas, M. M.; Rogers, R. D.; Mason, W. R. *Inorg. Chem.* **1989**, *28*, 1028 and references therein.
(5) Savas, M. M. Dissertation, Northern Illinois University, 1987.
(6) Harvey, P. D.; Gray, H. B. *J. Am. Chem. Soc.* **1988**, *110*, 2145.

0020-1669/89/1328-4366$01.50/0

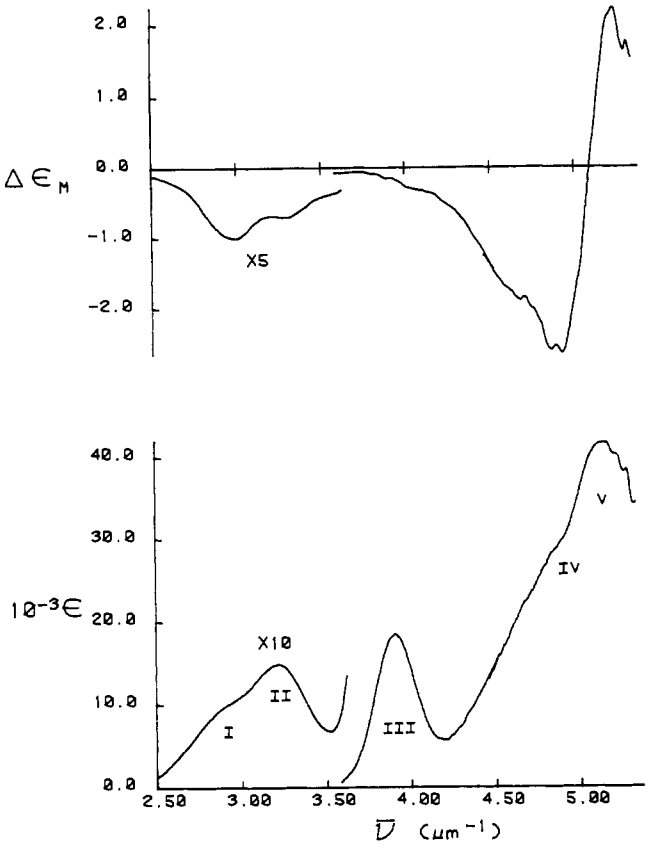

Figure 1. Absorption (lower curves) and MCD (upper curves) spectra for $[Au_2(dmpm)_3](ClO_4)_2$ in H_2O. The absorption and MCD data from 2.5–3.6 μm^{-1} were multiplied by factors of 10 and 5, respectively, before plotting.

used without further purification. The chloride salt, $[Au_2(dmpm)_3]Cl_2$, was prepared by following the published procedure[1] by treating $Au(PEt_3)Cl$[7] with 1.6 equiv of dmpm in dry acetone. The perchlorate salt, $[Au_2(dmpm)_3](ClO_4)_2$, was prepared by treating a suspension of $[Au_2(dmpm)_2](ClO_4)_2$[4] in dry acetone under N_2 with excess (8:1) dmpm. The ligand was added dropwise as the suspension was stirred, and a pale yellow solution formed. The solvent volume was reduced by evaporation in a stream of dry N_2, and ethyl ether was added to enhance precipitation. The solid was collected by filtration and recrystallized from 1:5 CH_3CN/MeOH. Both salts gave satisfactory elemental analysis, and both solids exhibit yellow fluorescence under UV light at room temperature. The solids are air stable and stable in neutral aqueous solution for several hours but lose 1 mol of dmpm/mol when treated with dilute acid, giving $Au_2(dmpm)_2^{2+}$. The solubility of the chloride salt in water is much greater than the perchlorate salt, but dilute solutions of the latter for spectral study could be prepared easily.

Spectral Measurements. Absorption spectra were obtained by using a Cary 1501 spectrophotometer. Spectra at 77 K were measured by immersing a PVA film containing $[Au_2(dmpm)_3]Cl_2$ into liquid N_2 in a quartz optical Dewar flask situated in the light beam of the spectrophotometer. Gaseous He was bubbled through the liquid N_2 above the sample to eliminate the boiling and therefore the light scattering in the vicinity of the sample. The PVA film samples were prepared by dissolving the gold salt in a 5% aqueous solution of PVA; the viscous solution was then spread in a thin layer on a glass plate and allowed to dry overnight. The solidified film was then carefully removed from the glass plate and checked for optical quality (low scattering and negligible birefringence) and solute absorbancy. In order to compensate for differences in background scattering, the 300 and 77 K PVA film spectra were superimposed in a low-energy region (~2.0 μm^{-1}) where absorption due to the solute was negligible. Measurements on pure PVA films showed that the scattering differences were virtually constant in the region 2.0–4.0 μm^{-1}.

Absorption and MCD spectra were determined simultaneously and synchronously along the same light path by means of a computer-controlled spectrometer described elsewhere.[8] A field of 7.0 T was provided by a superconducting magnet system (Oxford Instruments SM2-7, fitted with a room-temperature bore tube). All solution spectra were corrected for solvent blank. Beer's law was observed to hold within experimental error in the range of 3×10^{-5}–5×10^{-4} M for both CH_3CN and H_2O solutions.

Table I. Spectral Data for $[Au_2(dmpm)_3](ClO_4)_2$

	absorption			MCD	
band no.	$\bar{\nu}$, μm^{-1}	λ, nm	ϵ, M^{-1} cm^{-1}	$\bar{\nu}$, μm^{-1}	$\Delta\epsilon_M$, M^{-1} cm^{-1} T^{-1}
			In H_2O		
I	2.94	340.5	1070	2.98	−0.20
II	3.21	311.3	1490	3.27	−0.14
III	3.91	255.9	18500		
				4.02[a]	−0.29
				4.63[a]	−1.79
IV	4.86[a]	205.8	30000	4.89	−2.62
V	5.15	194.1	44000	5.09[b]	0
				5.24	+2.24
			In CH_3CN		
I	2.89	346.5	1060	2.95	−0.25
II	3.24	308.5	1600	3.30	−0.17
III	3.91	255.9	21500		
				4.10[a]	−0.45
				4.55[a]	−1.32
IV	4.85[a]	206.0	35000	4.86	−3.50
V	5.10	196.0	53000	5.11[b]	0

[a] Shoulder. [b] *A* term.

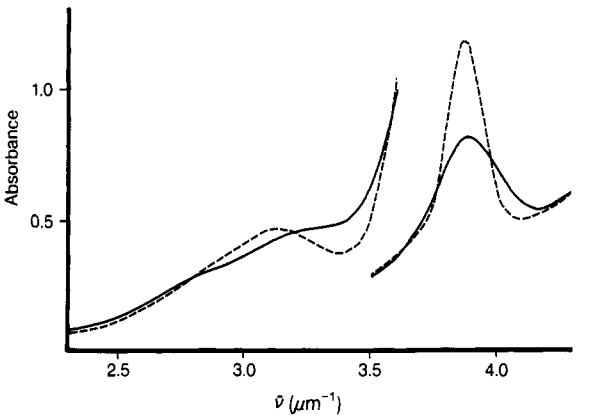

Figure 2. Absorption spectra at 300 K (—) and 77 K (---) for $[Au_2(dmpm)_3]Cl_2$ dissolved in aqueous PVA and solidified as thin films. The spectra on the left were of higher concentration that those on the right.

Results and Discussion

Figure 1 presents the absorption and MCD spectra for $[Au_2(dmpm)_3](ClO_4)_2$ in H_2O; the results for CH_3CN solution were of comparable quality except that the highest energy positive MCD feature was obscured by solvent absorption. The MCD spectrum shows a strong positive *A* term[9] for band V centered at 5.1 μm^{-1}, a poorly resolved negative shoulder for band IV, and weaker negative features corresponding to bands I and II. The MCD spectrum is unusually weak and poorly resolved in the vicinity of the intense band III near 3.9 μm^{-1}. This result is in contrast to the MCD spectrum of $Au_2(dmpm)_2^{2+}$, which shows an analogous intense band near 3.7 μm^{-1} (ϵ = 18400 M^{-1} cm^{-1}) with a well-defined and clearly resolved negative MCD *B* term. Quantitative absorption and MCD data are summarized in Table I. Absorption spectra at 300 and 77 K for $[Au_2(dmpm)_3]Cl_2$ dissolved in aqueous PVA and solidified to give thin films are shown in Figure 2. Measurement in the region of bands IV and V was not possible due to Cl^- and PVA absorption. The PVA spectra show that band III exhibits the characteristic low-temperature decrease in bandwidth and increase in maximum ab-

(7) Mann, F. G.; Wells, A. F.; Purdie, D. *J. Chem. Soc.* **1937**, 1828.
(8) Mason, W. R. *Anal. Chem.* **1982**, *54*, 646.
(9) For a detailed description of MCD spectroscopy along with the conventions in standard use, see: Piepho, S. B.; Schatz, P. N. *Group Theory in Spectroscopy with Applications to Magnetic Circular Dichroism*; Wiley-Interscience: New York, 1983.

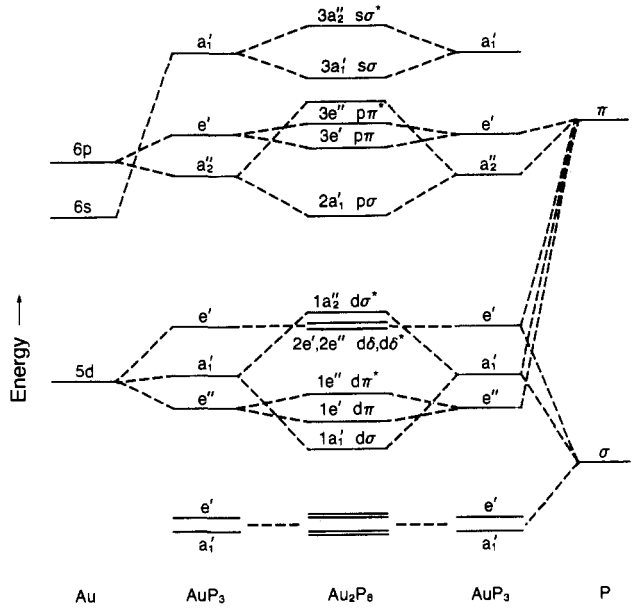

Figure 3. One-electron MO energy levels.

sorptivity expected for an allowed transition. Bands I and II appear to shift toward each other at low temperature so that band I is less well resolved, but the two bands do not decrease in intensity at low temperature and thus are not vibronic in origin.

Molecular Orbitals, Excited States, and MCD Terms. Figure 3 presents a schematic one-electron MO energy level diagram that will be suitable for visualizing the low-energy excited configurations and states necessary to interpret the absorption and MCD spectra. Although the molecular symmetry of the $Au_2(dmpm)_3^{2+}$ cation is lower (C_{3h}), the local symmetry imposed by the P donor atoms on the Au(I) ions in the Au_2P_6 complex approximates D_{3h}. Therefore, the levels of Figure 3 were constructed by assuming D_{3h} symmetry with the origin midway between the Au atoms, the z axis taken along the C_3 axis, and the y axis parallel to one eclipsed pair of Au–P bonds from the two AuP_3 units. Figure 3 also includes energy levels for the mononuclear D_{3h} AuP_3 unit (z axis perpendicular to the molecular plane, y axis along one Au–P bond) for comparison. The highest energy occupied level is for the Au_2P_6 complex either $1a_2''$ or $2e''$ and therefore the closed shell complex is diamagnetic and has a totally symmetric ground state designated $^1A_1'$. Dipole selection rules in D_{3h} dictate that only transitions to $^1E'$ (x,y-polarized) and $^1A_2''$ (z-polarized) excited states will be fully allowed. However, the spin–orbit coupling in the heavy Au(I) ions ($\zeta_{5d} \sim 0.4$–$0.5\ \mu m^{-1}$) will serve to intermix singlet and triplet excited states and allow transitions to states of triplet parentage to gain considerable intensity. Table II lists the states of the excited configurations expected to be lowest in energy. The symmetries of the spin–orbit states derived from the singlet and triplet states in the absence of spin–orbit interaction are also included in Table II. Excited configurations that give rise to symmetry-forbidden states $^{1,3}A_1'$, $^{1,3}A_2'$, $^{1,3}A_1''$, and $^{1,3}E''$ are not included in Table II; transitions to these states are expected to be orders of magnitude weaker than those to the symmetry-allowed E′ and A_2'' states.

MCD A terms, which result from a Zeeman splitting of degenerate levels, may be observed for the E′ states of $Au_2(dmpm)_3^{2+}$. A terms are described by the parameter ratio $\bar{A}_1/\bar{D}_0$ given in eq 1,[9] where the space-averaged case appropriate for

$$\bar{A}_1/\bar{D}_0 = \frac{-1}{\sqrt{2}\mu_B}\langle E'||\mu||E'\rangle \qquad (1)$$

nonisotropic molecules in solution is assumed, $\bar{D}_0 = {}^1/_3|\langle A_1'||\mathbf{m}||E'\rangle|^2$ is related to the dipole strength of the transition to the E′ state, μ_B = Bohr magneton, and $\mu \approx -\mu_B$ (L + 2S) and $\mathbf{m} = e\mathbf{r}$ are the magnetic and electric moment operators, respectively. By the approximation of the MO's of the excited configurations as pure 5d or 6p atomic orbitals of Au, the reduced matrix element (RME) of eq 1 can be evaluated and values of $\bar{A}_1/\bar{D}_0$ can be calculated for each E′ state; these values are included in Table II.

Table II. Excited Configurations and States

excited config[a]	zero-order states	spin–orbit states[b]	calcd $\bar{A}_1/\bar{D}_0$[c]
$(1a_2'')(2a_1')$	$^1A_2''$	A_2''	
	$^3A_2''$	(A_1''), E′	+2
$(2e')^3(2a_1')$	$^1E'$	E′	−2
	$^3E'$	(E'',A_1''), E′, A_2''	−2
$(1e')^3(2a_1')$	$^1E'$	E′	+1
	$^3E'$	(E'',A_1''), E′, A_2''	+1
$(2e'')^3(3e')$	$^1A_2''$	A_2''	
	$^3A_2''$	(A_1''), E′	+2
$(2e')^3(3e')$	$^1E'$	E′	−1
	$^3E'$	(E'',A_1''), E′, A_2''	−1
$(1a_2'')(3e'')$	$^1E'$	E′	+1
	$^3E'$	(E'',A_1''), E′, A_2''	+1
$(2e'')^3(3e'')$	$^1E'$	E′	−1
	$^3E'$	(E'',A_1''), E′, A_2''	−1
$(2e')^3(3e'')$	$^1A_2''$	A_2''	
	$^3A_2''$	(A_1''), E′	+2

[a] Notation as in Figure 3. Ground-state configuration = $...(2e')^4(2e'')^4(1a_2'')^2$, $^1A_1'$. Filled orbitals omitted, and symmetry-forbidden excited configurations not included. [b] Dipole-forbidden states in parentheses. [c] For E′ states using eq 1 (see text).

MCD B terms result from intermixing of states in the presence of the strong magnetic field. The nondegenerate A_2'' excited states may exhibit B terms by intermixing with E′ states; B terms are also expected for E′ states interacting with A_2'' states and other E′ states. The B term is described by the $\bar{B}_0$ parameter given in eq 2[9] for the example of an $A_2''(j)$ state interacting with states

$$\bar{B}_0[A_2''(j),E'(k)] = \mathrm{Re}\left[-\frac{2}{3\mu_B}\sum_k(\Delta W_{kj})^{-1} \times \langle A_2''(j)||\mu||E'(k)\rangle\langle A_1'||\mathbf{m}||A_2''(j)\rangle\langle E'(k)||\mathbf{m}||A_1'\rangle\right] \qquad (2)$$

$E'(k)$, where $\Delta W_{kj} = W(E'(k)) - W(A_2''(j))$, the energy difference between the two states, and the summation is over all states k. In practice the summation can frequently be reduced to only a few terms because the $(\Delta W_{kj})^{-1}$ term reduces the contribution from states that are widely separated in energy. Finally, it may be remarked that MCD C terms[9] will be zero because the complex is diamagnetic and will not exhibit ground-state Zeeman splitting.

Spectral Assignments and MCD Interpretation. The ordering of highest energy occupied MO's (HOMO's) for $Au_2(dmpm)_3^{2+}$ is not known for certain. However, as a consequence of the relative energies of the filled orbitals of the AuP_3 unit (assumed to be Au–P σ^*,e′ > Au–P $\pi_\perp$,a_1' and $\pi_\parallel$,e″) together with the reasonable assumption that the $d\sigma$–$d\sigma^*$ splitting will be larger than the $d\delta$–$d\delta^*$ or $d\pi$–$d\pi^*$ on the formation of the Au_2P_6 cluster, the most likely HOMO is either the $d\sigma^*$ $1a_2''$ or the $d\delta^*$,$d\delta$ pair 2e″,2e′ (see Figure 3). Similar reasoning leads to the placement of the Au_2P_6 $p\sigma$ orbital $2a_1'$ as the lowest energy unoccupied MO (LUMO) in Figure 3. The out-of-plane p_z orbital of the AuP_3 unit (Au–P $\pi_\perp$,a_2'') is expected to be lower in energy and more strongly affected by Au–Au interaction on formation of Au_2P_6 than will the in-plane p_{xy} orbitals of AuP_3(Au–P σ^*,e′). Therefore, the lowest energy excitation should be Au_2-localized and should be either $d\sigma^* \rightarrow p\sigma$ or $d\delta \rightarrow p\sigma$. Consequently, the lowest energy most intense bands are expected to involve transitions to the resulting spin–orbit states of predominantly singlet character, $A_2''(^1A_2'',1a_2'' \rightarrow 2a_1')$ or $E'(^1E',2e' \rightarrow 2a_1')$, respectively. The intensity of the transition to the E′ state however is expected to be very low due to a nearly zero electric moment (the AuP_3 excitation e′ → a_2'' from which the Au_2P_6 excitation is derived is actually symmetry-forbidden). In contrast, the $d\sigma^* \rightarrow p\sigma$ transition to A_2'' is expected to have a substantial electric moment and therefore to be prominent among the low-energy bands. For this reason band III at 3.91 μm^{-1} is assigned to the $d\sigma^* \rightarrow p\sigma$

transition to $A_2''(^1A_2'')$. The transition to the $E'(^1E')$ state expected close in energy is most certainly obscured by the intense absorption of band III. The strong $d\sigma^* \rightarrow p\sigma$ transition has emerged as a characteristic feature of closed-shell binuclear complexes which feature "nonbonded" metal–metal interaction. The related $Pt_2(dppm)_3$ complex (Pt–Pt distance 3.023 (1) Å[10]), for example, has an intense band at 2.05 μm^{-1} (77 K, 2-MeTHF solution)[6] assigned to this transition, and $Au_2(dmpm)_2^{2+}$ exhibits an intense band at 3.7 μm^{-1} (CH_3CN or H_2O solution) that was similarly assigned.[4] The marked red shift in the $d\sigma^* \rightarrow p\sigma$ transition from the Au_2^{2+} complex to the Pt_2 complex can be traced to a lower 5d–6p separation for Pt(0) ($\sim$2.6–3.0 μm^{-1}) compared to Au(I) ($\sim$5–6 μm^{-1}).[11] The energy difference for the transition between $Au_2(dmpm)_3^{2+}$ and $Au_2(dmpm)_2^{2+}$ is not very large, which is consistent with the Au_2-localized nature of the transition making it rather insensitive to the coordination environment about the Au(I) ions. It should be noted that the Au–Au distance, which should be a sensitive indicator of the extent of Au–Au interaction, is not very different in these two complexes (3.050 (1) Å for $Au_2(dmpm)_3^{2+}$ vs 3.028 (2) Å for $Au_2(dmpm_2^{2+})$.[1,4]

As noted above, there is a marked difference in the weak, poorly resolved MCD signal in the region of band III for $Au_2(dmpm)_3^{2+}$ and the well-resolved negative *B* term observed earlier[4] for $Au_2(dmpm)_2^{2+}$. In order to explain this difference, an effort was made to calculate $\bar{B}_0$ for the $A_2''(^1A_2'')$ state by using eq 2. A number of close-lying E′ states were considered (all those of Table II plus several higher in energy). When the appropriate one-electron D_{3h} MO's were formulated (approximated as 5d or 6p Au atomic orbitals), the $\langle A_2''||\mu||E'(k)\rangle$ reduced matrix elements either were zero in a one-centered approximation or were expected to be very small in a two-centered treatment. For example, the $\langle A_2''(^1A_2'')||\mu||E'(^1E')\rangle$ RME for the coupling of states from the close lying $d\sigma^* \rightarrow p\sigma$ and $d\delta \rightarrow p\sigma$ transitions discussed above is zero because the RME reduces to the one-electron integrals $\langle d_{z^2}|\mu|d_{x^2-y^2}\rangle = \langle d_{z^2}|\mu|d_{xy}\rangle$, which are zero in a one-centered approximation. In contrast, several important one-centered terms are *non*zero for the lower symmetry (D_{2h}) $Au_2(dmpm)_2^{2+}$ complex.[4] Therefore, the weak, poorly resolved MCD signal for band III for the trigonal complex can be traced to orbital restrictions on the magnetic coupling between the A_2'' state and the various close-lying E′ states. It should be remarked, however, that *B*-term arguments of the sort given here and earlier[4] must be viewed with caution, especially if the detailed placement of individual states is not known for certain, but in the present case the orbital restrictions to a first approximation are clear and predict a result that is consistent with experiment.

The weaker bands I and II found to lower energy of band III (see Figures 1 and 2) can logically be assigned as transitions to spin–orbit states of predominantly triplet parentage. If the $d\sigma^* \rightarrow p\sigma$ transitions were the only low-energy excitations, then only a single allowed transition to the $E'(^3A_2'')$ state would be anticipated in this energy region (the A_1'' excited state of the $1a_2''2a_1'$ configuration is symmetry-forbidden). The observation of two bands in the 2.5–3.5-μm^{-1} region argues convincingly for the presence of a state from another excited configuration. As discussed above, the $d\delta \rightarrow p\sigma$ excitation is expected at energies similar to those of $d\sigma^* \rightarrow p\sigma$. Among the excited states of the $(2e')^3(2a_1')$ configuration is the symmetry-allowed $A_2''(^3E')$ state (see Table II). Therefore, on the basis of singlet–triplet separation energies (typically 0.3–0.6 μm^{-1}), band II is assigned as the transition to $E'(^3A_2'')$ and band I is assigned as the transition to $A_2''(^3E')$. The reverse assignment of these two bands is less reasonable due to the larger separation of the $E'(^3A_2'')$ state from the $A_2''(^1A_2'')$ state (band III) of the same excited configuration ($\sim$0.9–1.0 μm^{-1}). The MCD spectrum in the 2.5–3.5-μm^{-1} region is unfortunately not very informative, since it shows only two broad negative features for bands I and II. Band II should have a positive *A* term if the assignment is correct, but the *A* term could easily be obscured by its own *B* term and from overlapping contributions from band I. It might be noted that the MCD minimum for band II does not correspond with the absorption maximum (see Figure 1 and Table I), which signals a complex MCD band shape that could result from *A*- and *B*-term contributions. Finally, the two lowest energy bands observed for the related $Pt_2(dppm)_3$ complex[6] are weaker than the $d\sigma^* \rightarrow p\sigma$ singlet band and have been assigned the same way as bands I and II for $Au_2(dmpm)_3^{2+}$ here.

The highest energy bands observed in the absorption spectrum, bands IV and V, which are not well resolved (see Figure 1), indicate the presence of two (or more) strongly allowed transitions to excited states close in energy. The MCD spectrum is similarly unresolved but is dominated by the strong positive *A* term. It is likely that both bands IV and V involve transitions to E′ states that have positive *A* terms, otherwise a more complicated MCD band shape would be expected. Two plausible candidates are transitions to the $E'(^1E')$ states of the $(1a_2'')(3e'')$ configuration (band V) and the $(1e')^3(2a_1')$ configuration (band IV). Both of these E′ states are expected to have positive *A* terms from eq 1 (see Table II). Although the present results are not able to provide a definite placement of one of these states lower in energy than the other, the choice suggested is based on consistency with related states proposed recently for $Au_2(dmpm)_2^{2+}$.[4] Nevertheless, both of the E′ states are mainly AuP_3 localized and represent intense Au–P $d\sigma^* \rightarrow p\sigma^*$ and $d\pi \rightarrow p\pi$ (out of plane) transitions, respectively. It should be noted that the other $E'(^1E')$ states of Table II from the $(2e')^3(3e')$ and $(2e'')^3(3e'')$ configurations can be ruled out because they each predict negative *A* terms, contrary to experiment. It is interesting that the related $Pt_2(dppm)_3$ complex also exhibits two intense bands near 3.3 μm^{-1} and higher in energy than the $d\sigma^* \rightarrow p\sigma$ band.[6] Although these bands were not assigned previously, it is likely that an interpretation analogous to that proposed here for $Au_2(dmpm)_3^{2+}$ would apply.

Concluding Remarks. The spectral assignments proposed here and the interpretation of the MCD spectra for $Au_2(dmpm)_3^{2+}$ are consistent with previous assignments of the related $Pt_2(dppm)_3$ and $Au_2(dmpm)_2^{2+}$ complexes.[4,6] In fact, the pattern exhibited by the absorption spectra of all three complexes is remarkably similar. Each shows a low-energy intense $d\sigma^* \rightarrow p\sigma$ M_2-localized transition with one or more weaker transitions to states of spin-forbidden parentage to the red region, and each shows higher energy intense bands that can be associated with MP_3- (M = Au, Pt) or AuP_2-localized transitions. The energy difference between the Pt_2 and Au_2^{2+} $d\sigma^* \rightarrow p\sigma$ that the M_2-localized transition is sensitive to metal oxidation state and metal orbital stability. In contrast, the similarity of band energies for the $d\sigma^* \rightarrow p\sigma$ transition between $Au_2(dmpm)_3^{2+}$ and $Au_2(dmpm)_2^{2+}$ reflects the low sensitivity of the Au–Au interaction to the coordination environment about the Au(I) ions. The coordination environment does however affect the magnetic interaction between excited states, and the MCD spectrum is a sensitive probe of this effect. The $5d^{10}$–$5d^{10}$ metal–metal interaction in the binuclear Pt_2 and Au_2^{2+} complexes is believed to be relativistic in origin.[4,12] The mixing of the relativistic 6s, and to a lesser extent 6p, orbitals with the $d\sigma$ and $d\sigma^*$ orbitals of the binuclear complex is expected to provide a stabilization of the ground state.

Acknowledgment is made to the donors of the Petroleum Research Fund, administered by the American Chemical Society, for support of this work.

(10) Manojlovic-Muir, L.; Muir, K. W. *J. Chem. Soc., Chem. Commun.* **1982**, 1155. Manojlovic-Muir, L.; Muir, K. W.; Grossel, M. C.; Brown, M. P.; Nelson, C. D.; Yavari, A.; Kallas, E.; Moulding, R. P.; Seddon, K. R. *J. Chem. Soc., Dalton Trans.* **1986**, 1955.

(11) Moore, C. E. *Natl. Bur. Stand. Circ. (U.S.)* **1958**, *No. 467*, Vol. III.

(12) Pyykkö, P. *Chem. Rev.* **1988**, *88*, 563.